Electronic Supplementary Material (ESI) for Dalton Transactions.
This journal is © The Royal Society of Chemistry 2020

Supporting Information

Construction of Novel Luminescent Lanthanide Framework for Selective Sensing of Cu^{2+} and 4-Nitrophenol in water

Zeng-Gang Lin,[a] Fu-Qiang, Song,[a] Hui, Wang,[a] Xue-Qin, Song,[a]* Xin-Xin, Yu,[a] and Wei-sheng Liu[b]

a) School of Chemical and Biological Engineering, Lanzhou Jiaotong University, Lanzhou 730070, China

b) College of Chemistry and Chemical Engineering and State Key Laboratory of Applied Organic Chemistry, Lanzhou University, Lanzhou 730000, China

Contents

Materials and Physical Measurements ----------S3

Details of Single Crystal X-ray Diffraction ----------S3~S4

Table S1 Crystal data and structure refinement parameters for **LZG-Eu** and **LZG-Tb** ---------S5

Table S2 Shape calculation results of **LZG-Eu** and **LZG-Tb** ----------S5

Table S3 Important bond lengths and angels for **LZG-Eu** and **LZG-Tb**----------S6

Fig. S1 IR spectra of $\mathbf{H_4L}$, **LZG-Eu** and **LZG-Tb** ----------S7

Fig. S2 TGA curves of **LZG-Eu** and **LZG-Tb** under N_2 atmosphere from 30 to 800 ℃.----------S7

Fig. S3 Powder X-ray diffraction patterns (PXRD) of **LZG-Eu** and **LZG-Tb** and that of simulated from single crystal analysis.----------S7

Fig. S4 PXRD patterns of **LZG-Eu** after treated by aqueous solutions with various pH values from 3 to 12, after storage in water for 14 days, after frozen at -20℃ and heated at 50℃ in water for 1 day.----------S8

Fig. S5 PXRD patterns of **LZG-Tb** after treated by aqueous solutions with various pH values from 3 to 12, after storage in water for 14 days, after frozen at -20℃ and heated at 50℃ in water for 1 day.----------S8

Fig. S6 The relative emission intensity of **LZG-Eu** (a) and **LZG-Tb** (b) in aqueous solutions with different pH values (3-12) and different temperatures.----------S9

Fig. S7 The projection structure and topology of **LZG-Tb** ----------S9

Fig. S8 The N_2 adsorption isotherms of **LZG-Tb** at 195 K ----------S9

Fig. S9 Excitation and emission spectra of **H_4L**----------S10

Fig. S10 The luminescence decay lifetimes of the **LZG-Eu**(a) and **LZG-Tb**(b) ----------S10

Fig. S11 The competition experiments of **LZG-Eu** (a) and **LZG-Tb** (b) for the detection of Cu^{2+} ion in the presence of the interference metal cations----------S10

Fig. S12 The competition experiments of **LZG-Eu** (a) and **LZG-Tb** (b) for the detection of 4-NP in the presence of the interference nitro explosives----------S11

Fig. S13 PXRD patterns of **LZG-Eu**, **LZG-Tb** after storage in 4-NP and Cu^{2+} aqueous solutions.----------S11

Fig. S14 a) The decay curves of **LZG-Eu** water suspension under different concentrations of 4-NP; b) Excitation spectra of **LZG-Eu** water suspensions under different concentrations of 4-NP; c) Excitation spectra of **LZG-Tb** water suspensions under different concentrations of 4-NP-------S11

Fig. S15 a) The luminescence response of **LZG-Eu** to different concentrations of Cu^{2+}(0~0.60μM) in river water. b) The relationship between the I_0/I Stern-Volmer diagram of **LZG-Eu** and the increase of Cu^{2+} concentration in river water. c) The luminescence response of **LZG-Tb** to different concentrations of Cu^{2+}(0~1.0μM) in river water. d) The relationship between the I_0/I Stern-Volmer diagram of **LZG-Tb** and the increase of Cu^{2+} concentration in river water.----------S12

Fig. S16 a) The luminescence response of **LZG-Eu** to different concentrations of 4-NP(0~7.5 μM) in river water. b) The relationship between the I_0/I Stern-Volmer diagram of **LZG-Eu** and the increase of 4-NP concentration in river water. c) The luminescence response of **LZG-Tb** to different concentrations of 4-NP(0~7.5μM) in river water. d) The relationship between the I_0/I Stern-Volmer diagram of **LZG-Tb** and the increase of 4-NP concentration in river water.---------- S13

Fig. S17 a) The luminescence response of **LZG-Eu** to different concentrations of Cu^{2+}(0-0.65μM) in tap water; b) The relationship between the I_0/I Stern-Volmer diagram of **LZG-Eu** and the increase of Cu^{2+} concentration in tap water; c) The luminescence response of **LZG-Tb** to different concentrations of Cu^{2+}(0-1.0μM) in tap water; d) The relationship between the I_0/I Stern-Volmer diagram of **LZG-Tb** and the increase of Cu^{2+} concentration in tap water.----------S14

Fig. S18 a) The luminescence response of **LZG-Eu** to different concentrations of 4-NP(0-7.5μM) in tap water; b) The relationship between the I_0/I Stern-Volmer diagram of **LZG-Eu** and the increase of 4-NPconcentration in tap water; c) The luminescence response of **LZG-Tb** to different concentrations of 4-NP(0-7.5μM) in tap water; d) The relationship between the I_0/I Stern-Volmer diagram of **LZG-Tb** and the increase of 4-NP concentration in tap water.----------S15

References----------S15

Materials and Physical Measurements

All the reagents and $Ln(NO_3)_3 \cdot 6H_2O$ used were purchased from Aladdin Reagent (Shanghai) Co., Ltd. without further purification.

The relevant data of the elemental analysis described in this article was obtained through the Thermo Flash 2000 elemental analyzer. The infrared spectrum were measured on a Therrno Mattson FTIR spectrometer, and the wavenumber range was 4000~400 cm^{-1}. The powder X-ray diffraction (PXRD) patterns were determined on an X-ray diffractometer (Rigaku D/Max 2200PC) in the 2θ range of 5°~50°. The thermal analysis is performed from 30°C to 800°C at a heating rate of 10°C min^{-1} under N_2 atmosphere on a TGA/NETZSCH STA449C instrument. Nitrogen (N_2) gas sorption measurement was performed on a ASAP2020M&TriStar 3020 surface area analyzer (Micromeritics Instruments Corp., U.S.) at 195 K. The X-ray photoelectron spectroscopy (XPS) measurements were performed on Kratos AXIS Ultra DLD spectrometer. Mercury program version 3.10 were used to simulate the PXRD mode of rare earth complexes. F-7000 fluorescence spectrophotometer was used to obtain the luminescence of the solid powder and the suspension, and the wavelength range was 200~800 nm. The luminescence lifetime and quantum yield were recorded on the FLS920 luminescence spectrometer in Edinburgh instrument. The decay curves were fitted by a mono-exponential function: $I = I_0 + A\exp(-t/\tau)$, where I and I_0 are the luminescent intensities at time t = t and t = 0, respectively, and τ is defined as the luminescent lifetime. The luminescence quantum yields of the solid samples were determined by the absolute method using the integrating sphere on FLS920 (diameter 150 mm, BaSO4 coating) of Edinburgh Instrument.

Crystallographic Data Collection and Refinement.

Single crystals of **LZG-Eu** and **LZG-Tb** with approximate dimensions of 0.18 × 0.12 × 0.10 mm^3 and 0.20 × 0.16 × 0.14 mm^3 which were suitable for X-ray diffraction were obtained in moderate yield by solvothermal method. Crystal data of **LZG-Eu** was collected on a Bruker APEX-II CCD diffractometer (MoKα radiation, λ = 0.71073 Å) at 100 K and that for **LZG-Tb** was collected on a Bruker SuperNova diffractometer (CuKα radiation, λ = 1.54184 Å) at 293 K. Structures were solved by direct methods and refined by a full matrix least-squares technique based on F^2 using the SHELXL 2014 program.[1] All of the non-hydrogen atoms were refined anisotropically. The organic hydrogen atoms were generated geometrically. Disordered phenylic H and uncoordinated carboxyl H for **LZG-Eu** and uncoordinated carboxyl H for **LZG-Tb** were

not located but are included in their formulas. In addition, the disordered crystalline water and DMF molecules in **LZG-Eu** and **LZG-Tb** are difficult to identify, correspondingly, solvate molecules were accounted for by using the program PLATON/SQUEEZE (Spek, 2009) in order to remove the contributions of disordered solvent.[2] For details about the squeezed material, see cif data in Supporting Information. Therefore, free water and DMF molecules which were determined on the basis of TGA and elemental microanalysis, and the data treated with the SQUEEZE routine within PLATON were added to the molecular formula of **LZG-Eu** and **LZG-Tb** respectively. Drawings of the molecules were performed with the program Diamond.[3] Crystallographic data as well as details of data collection and refinement for these complexes are summarized in Table S1, important bond lengths are listed in Table S3. CCDC 2034442 and 2034444 contain the supplementary crystallographic data of **LZG-Eu** and **LZG-Tb**, which can be obtained from the authors or the Cambridge Crystallographic Data Centre via www. ccdc.cam.ac.uk/data_request/cif.

Table S1. Crystal data and structure refinement parameters for **LZG-Eu** and **LZG-Tb**.

CCDC No	2034442	2034444
Empirical formula	$C_{20}H_8N_2O_8Eu$	$C_{20}H_8N_2O_8Tb$
Temperature (K)	100(2)	293(2)
formula_weight	555.24	563.20
Diffraction	Mo Kα (0.71073 Å)	CuKα (1.54184 Å)
Crystal system, Space group	Trigonal, $P\bar{3}c1$	Trigonal, $P\bar{3}c1$
	a = 30.8375(8)Å; α =90°	a =30.5392(7)Å; α =90°
Unit cell dimensions	b = 30.8375(8)Å; β =90°	b =30.5392(7)Å; β =90°
	c = 12.9766(5)Å; γ = 120°	c =13.0003(4) Å; γ =120°
V/Å^3, Z	10686.8(7),12	10500.3(6), 12
D_{calcd}/Mg m^{-3}	1.035	1.069
μ/mm^{-1}	1.789	10.203
F(000)	3204	3252
Θ range for data collection	2.228°~27.534°	4.423° ~70.344°
	-39 ≤ *h* ≤ 40	-26≤ *h* ≤ 36
index ranges, *hkl*	-40 ≤ *k* ≤ 33	-36 ≤ *k* ≤ 26
	-16 ≤ *l* ≤ 16	-15 ≤ *l* ≤ 13
Independent reflections (R_{int})	0.0522	0.0515
Completeness	100 %	97.7%
Reflections unique / collected	8222 / 151590	6545 / 24811
Data / restraints / params	8222 / 70 / 298	6545 / 200 / 306
Goodness–of–fit on F^2	1.042	1.044
Final *R* indices [$I > 2\sigma(I)$][a,b]	R_1 =0.0675, wR_2 =0.1872	R_1 = 0.0450, wR_2 = 0.1160
R indices (all data)[a,b]	R_1 = 0.0685, wR_2 = 0.1879	R_1 = 0.0586, wR_2 = 0.1234

[a]$R_1 = \sum||F_o| - |F_c||/\sum|F_o|$. [b]$wR_2 = \{\sum[w (F_o^2 - Fc^2)^2]/ \sum[w (F_o^2)^2]\}^{1/2}$

S H A P E v2.1 Continuous Shape Measures calculation

(c) 2013 Electronic Structure Group, Universitat de Barcelona Contact: llunell@ub.edu

---

Table S2. Shape calculation results of Ln^{III} in **LZG-Eu** and **LZG-Tb**

	LZG-Eu	**LZG-Tb**
Octagon(OP-8)	0.27179	0.23509
Heptagonal pyramid(HPY-8)	0.17760	0.17438
Hexagonal bipyramid(HBPY-8)	0.19547	0.19737
Cube(CU-8)	0.21151	0.21179
Square antiprism(SAPR-8)	0.16282	0.16263
Triangular dodecahedron(TDD-8)	0.15185	0.14865
Johnson gyrobifastigium J26(JGBF-8)	0.20258	0.19825
Johnson elongated triangular bipyramid J14(JETBPY-8)	0.21950	0.21408
Biaugmented trigonal prism J50 (JBTPR-8)	0.16962	0.15230
Biaugmented trigonal prism (BTPR-8)	0.15528	0.14721
Snub diphenoid J84(JSD-8)	0.18026	0.17145
Triakis tetrahedron(TT-8)	0.21345	0.21379
Elongated trigonal bipyramid(ETBPY-8)	0.27311	0.26712

Table S3. Selected bond lengths (Å) and angles (°) for **LZG-Eu** and **LZG-Tb**.

{[Eu(HL]·3DMF·3H_2O}$_n$ (**LZG-Eu**)												
Eu1–O1	2.298(6)	Eu1–O2	2.416(5)	Eu1–O4	2.423(6)	Eu1–O5	2.308(6)	Eu1–O6	2.453(5)			
Eu1–O7	2.431(6)	Eu1–N1	2.494(6)	Eu1–N2	2.520(6)							
O1–Eu1–O4	79.8(2)	O1–Eu1–O5	121.0(3)	O1–Eu1–O6	81.7(2)	O1–Eu1–N1	138.4(3)					
O1–Eu1–N2	75.0(2)	O1–Eu1–O2	147.3(2)	O1–Eu1–O7	84.3(3)	O2–Eu1–O4	128.1(2)					
O2–Eu1–O6	1.40(18)	O2–Eu1–O7	84.22(19)	O2–Eu1–N1	64.6(2)	O2–Eu1–N2	72.4(2)					
O4–Eu1–O6	143.7(2)	N1–Eu1–N2	120.2(2)	O7–Eu1–N2	64.4(2)	O7–Eu1–N1	71.6(2)					
O7–Eu1–O6	127.82(18)	O6–Eu1–N2	63.40(17)	O6–Eu1–N1	139.75(18)	O5–Eu1–N2	135.4(2)					
O5–Eu1–N1	72.2(2)	O5–Eu1–O7	148.8(2)	O5–Eu1–O6	77.33(19)	O5–Eu1–O4	85.9(3)					
O5–Eu1–O2	81.9(2)	O4–Eu1–N2	138.6(2)	O4–Eu1–N1	63.6(2)	O4–Eu1–O7	81.0(3)					
{ [Tb(HL]·3DMF·3H_2O}$_n$ (**LZG-Tb**)												
Tb1–O2	2.379(4)	Tb1–O3	2.443(3)	Tb1–O4	2.275(4)	Tb1–O5	2.387(3)	Tb1–O6	2.268(4)			
Tb1–O7	2.382(4)	Tb1–N1	2.489(4)	Tb1–N2	2.483(4)							
O7–Tb1–N2	63.80(13)	O7–Tb1–N1	139.41(5)	O7–Tb1–O5	128.52(12)	O7–Tb1–O3	141.92(13)					
O6–Tb1–N2	139.88(15)	O6–Tb1–N1	76.68(15)	O6–Tb1–O7	79.67(5)	O6–Tb1–O5	148.38(14)					
O6–Tb1–O4	114.57(18)	O6–Tb1–O3	79.75(14)	O6–Tb1–O2	86.90(15)	N1–Tb1–N2	120.97(3)					
O5—Tb1–N2	64.73(12)	O5–Tb1–N1	72.08(13)	O5–Tb1–O3	82.35(12)	O4–Tb1–N2	79.06(15)					
O4–Tb1–N1	135.92(5)	O4–Tb1–O7	84.06(16)	O4–Tb1–O5	85.68(17)	O4–Tb1–O3	75.94(13)					
O4–Tb1–O2	151.73(15)	O3–Tb1–N2	139.80(2)	O3–Tb1–N1	63.97(12)	O2–Tb1–N2	72.73(13)					
O2–Tb1–N1	64.36(13)	O2–Tb1–O7	81.97(14)	O2–Tb1–O5	84.01(13)	O2–Tb1–O3	128.29(12)					

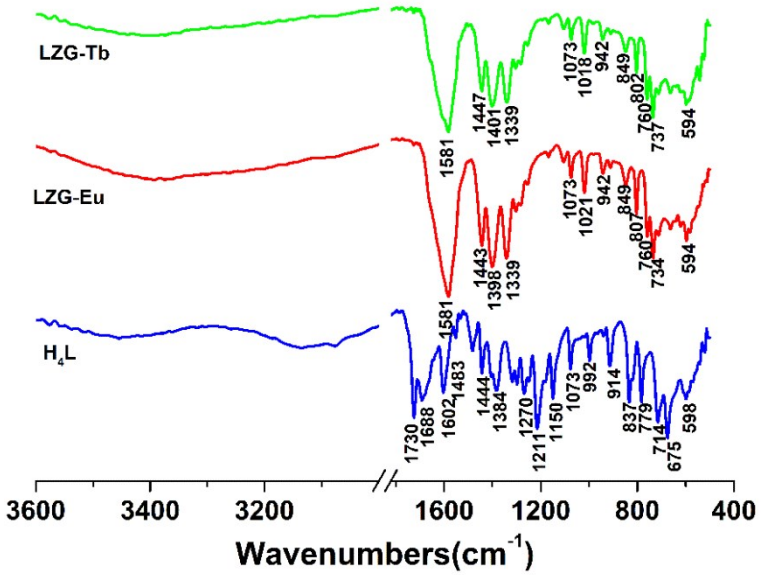

Fig. S1 IR spectra of **H_4L**, **LZG-Eu** and **LZG-Tb** in solid state.

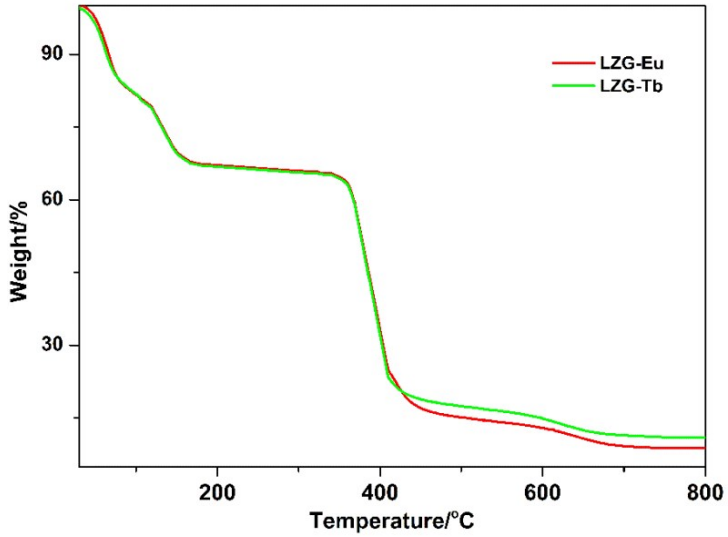

Fig. S2 TGA curves of **LZG-Eu** and **LZG-Tb** under N_2 atmosphere from 30 to 800 ℃.

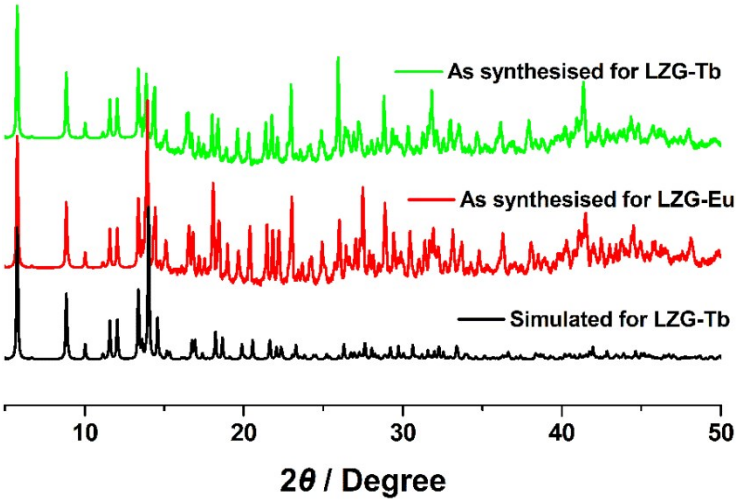

Fig. S3 Powder X-ray diffraction patterns (PXRD) of **LZG-Eu** and **LZG-Tb** and that of simulated from single crystal analysis.

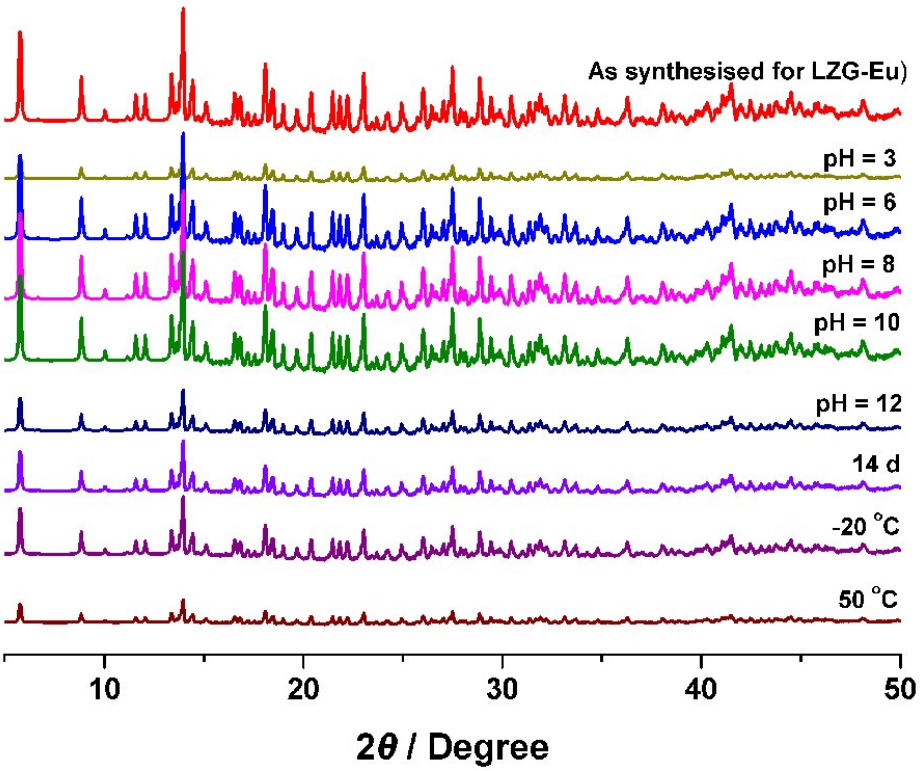

Fig. S4 PXRD patterns of **LZG-Eu** after treated by aqueous solutions with various pH values from 3 to 12, after storage in water for 14 days, after frozen at -20℃ and heated at 50℃ in water for 1 day.

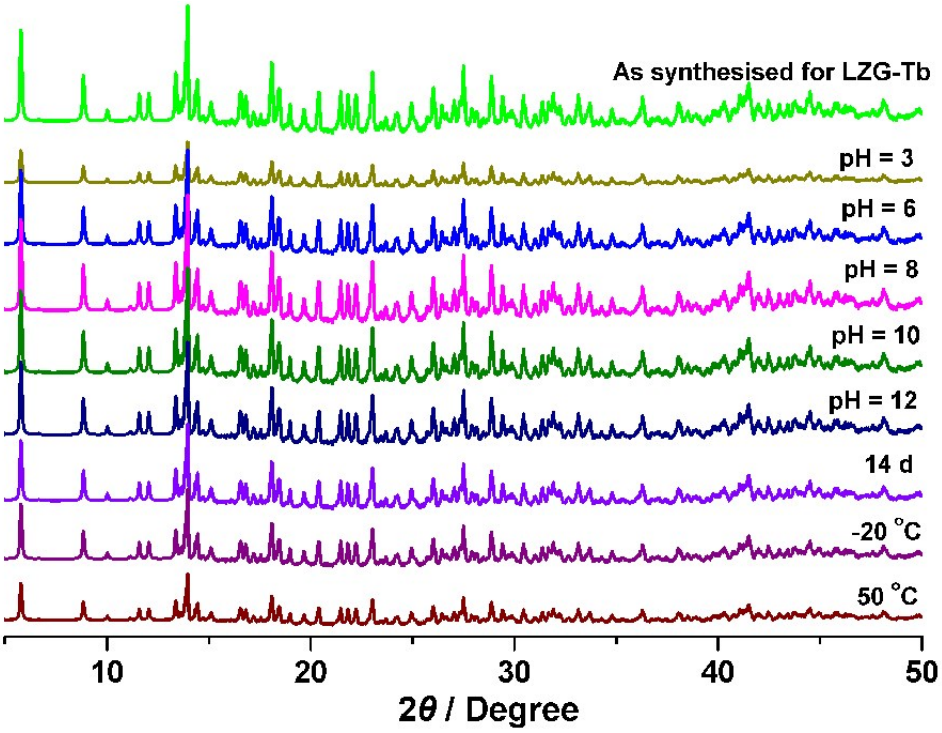

Fig. S5 PXRD patterns of **LZG-Tb** after treated by aqueous solutions with various pH values from 3 to 12, after storage in water for 14 days, after frozen at -20℃ and heated at 50℃ in water for 1 day.

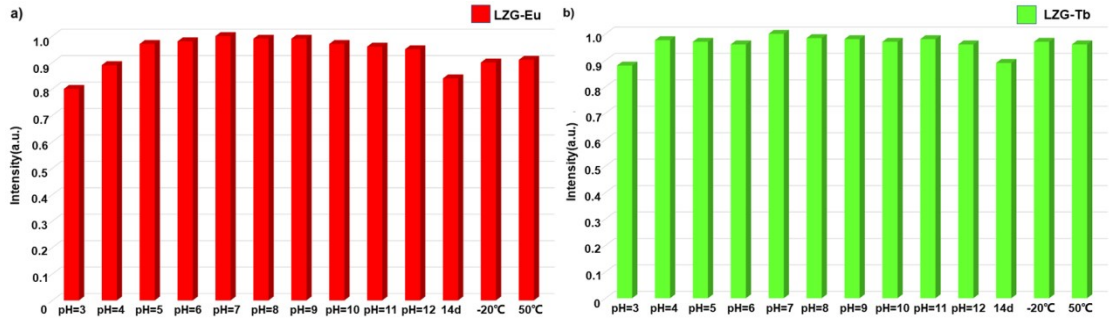

Fig. S6 The relative emission intensity of **LZG-Eu** at 614 nm (a) and **LZG-Tb** in 546 nm (b) in aqueous solutions with different pH values (3-12) and different temperatures.

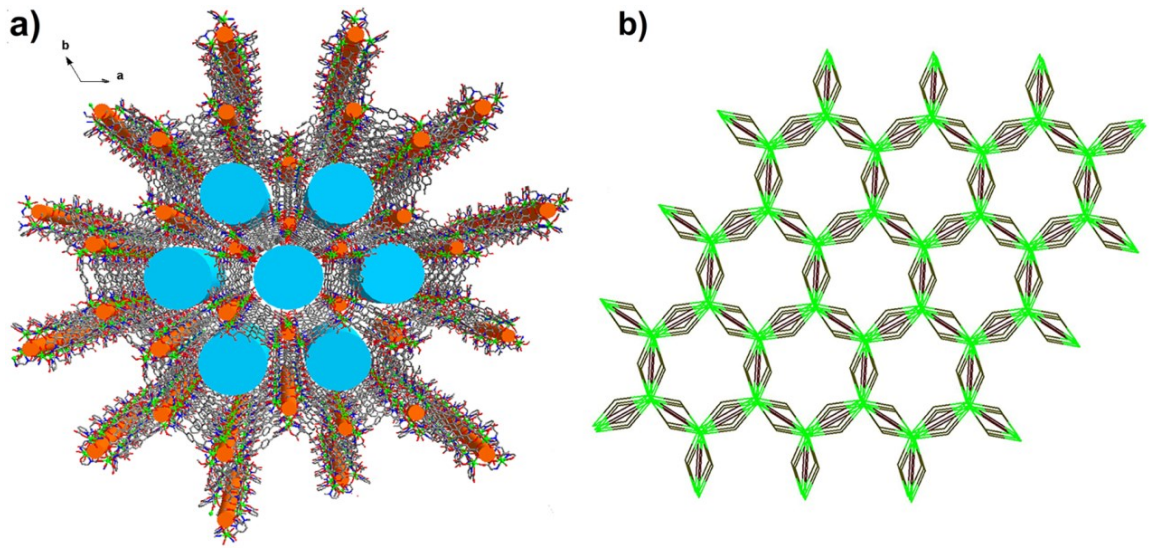

Fig. S7 The projection structure (a) and topology (b) of **LZG-Tb**.

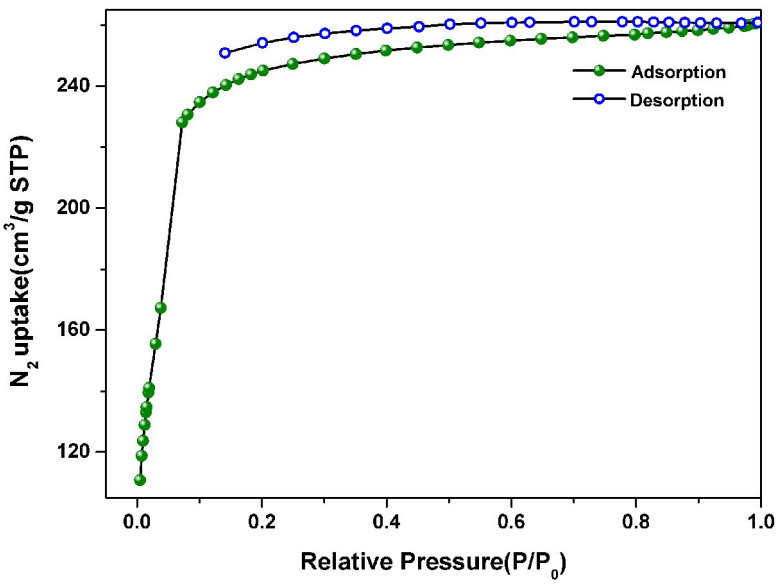

Fig. S8 The N_2 adsorption isotherms of **LZG-Tb** at 195 K.

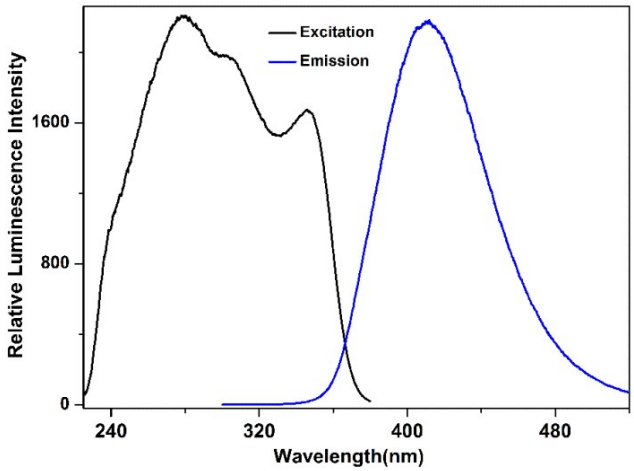

Fig. S9 Excitation and emission spectra of H_4L.

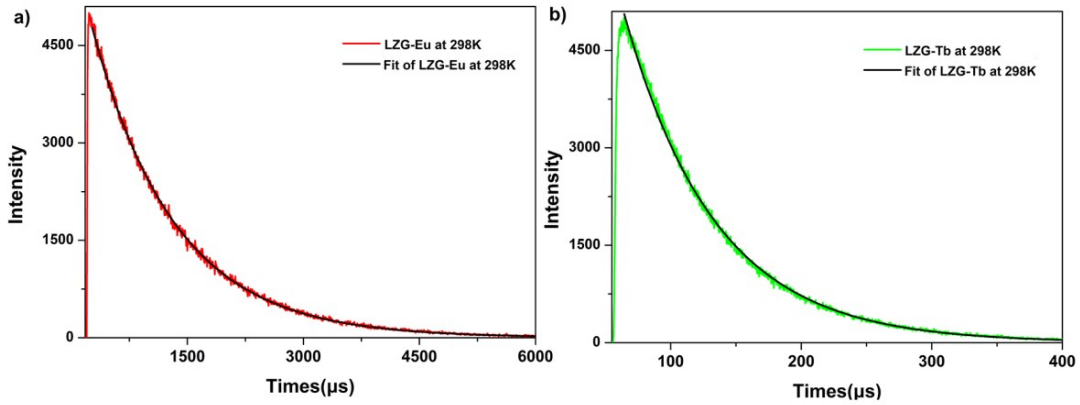

Fig. S10 The luminescence decay lifetimes of the **LZG-Eu**(a) and **LZG-Tb**(b).

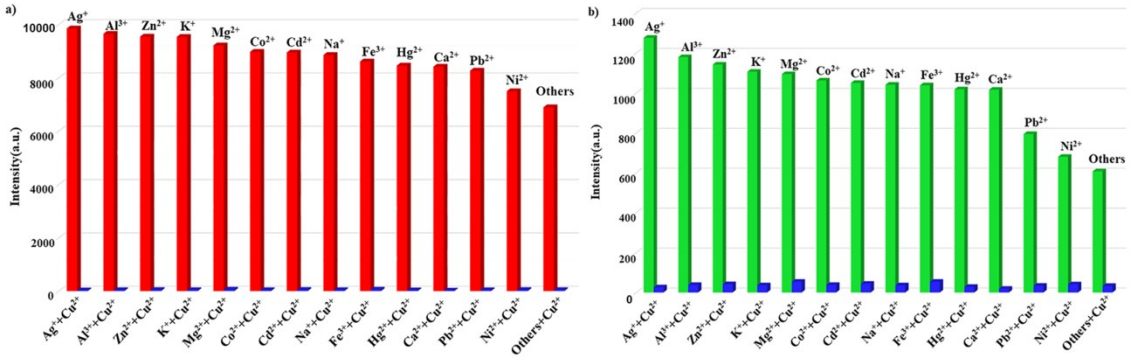

Fig. S11 The competition experiments of **LZG-Eu** (a) and **LZG-Tb** (b) for detection of Cu^{2+} ion in the presence of the interference metal cations.

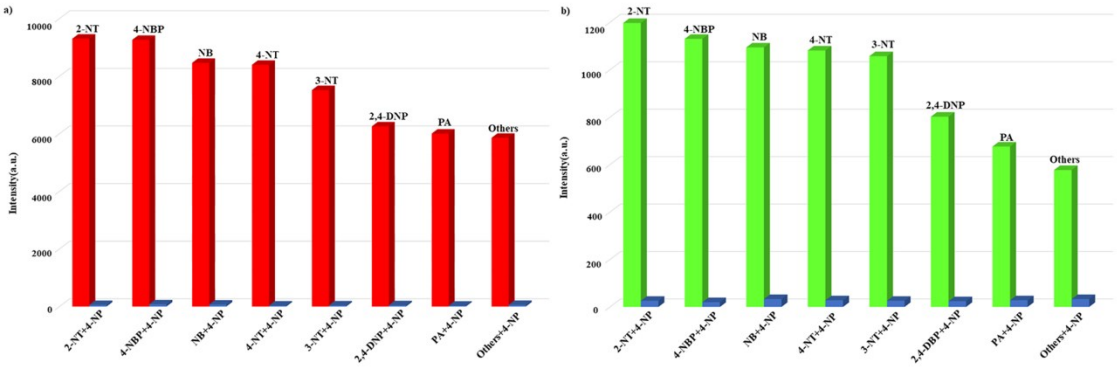

Fig. S12 The competition experiments of **LZG-Eu** (a) and **LZG-Tb** (b) for the detection of 4-NP in the presence of the interference nitro explosives.

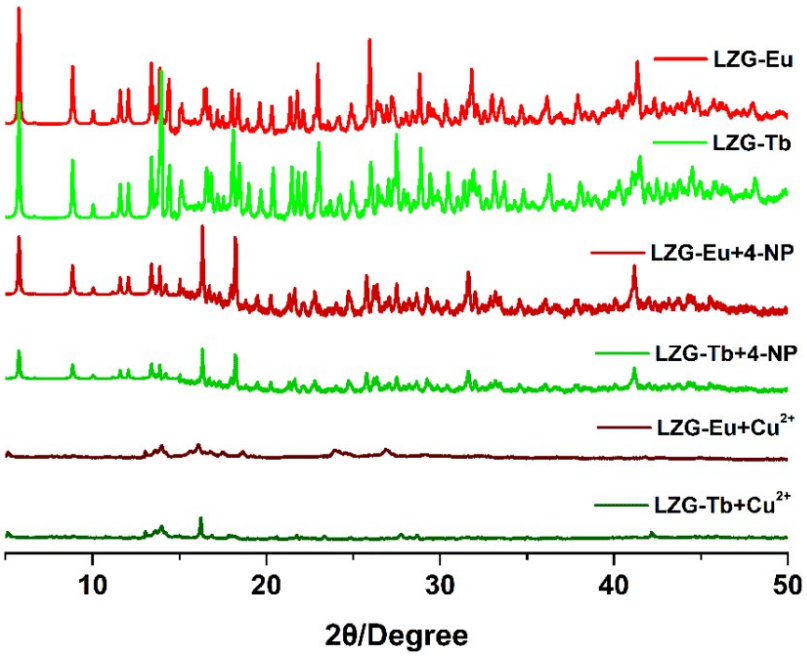

Fig. S13 PXRD patterns of **LZG-Eu**, **LZG-Tb** after immersed in 4-NP and Cu^{2+} aqueous solutions.

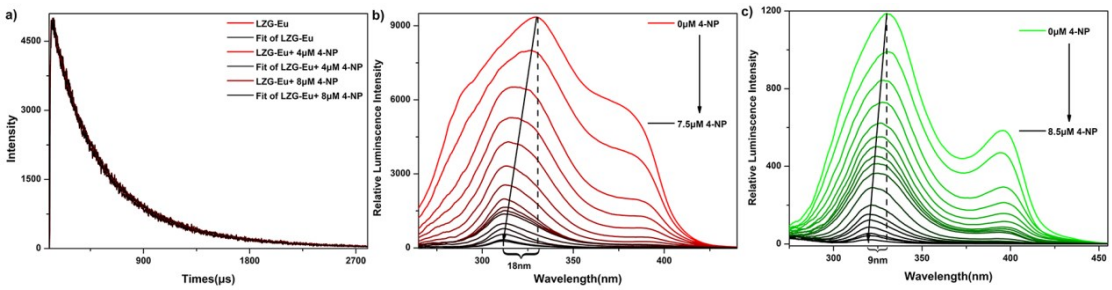

Fig. S14 a) The decay curves of **LZG-Eu** water suspension under different concentrations of 4-NP; b) Excitation spectra of **LZG-Eu** water suspensions under different concentrations of 4-NP; c) Excitation spectra of **LZG-Tb** water suspensions under different concentrations of 4-NP.

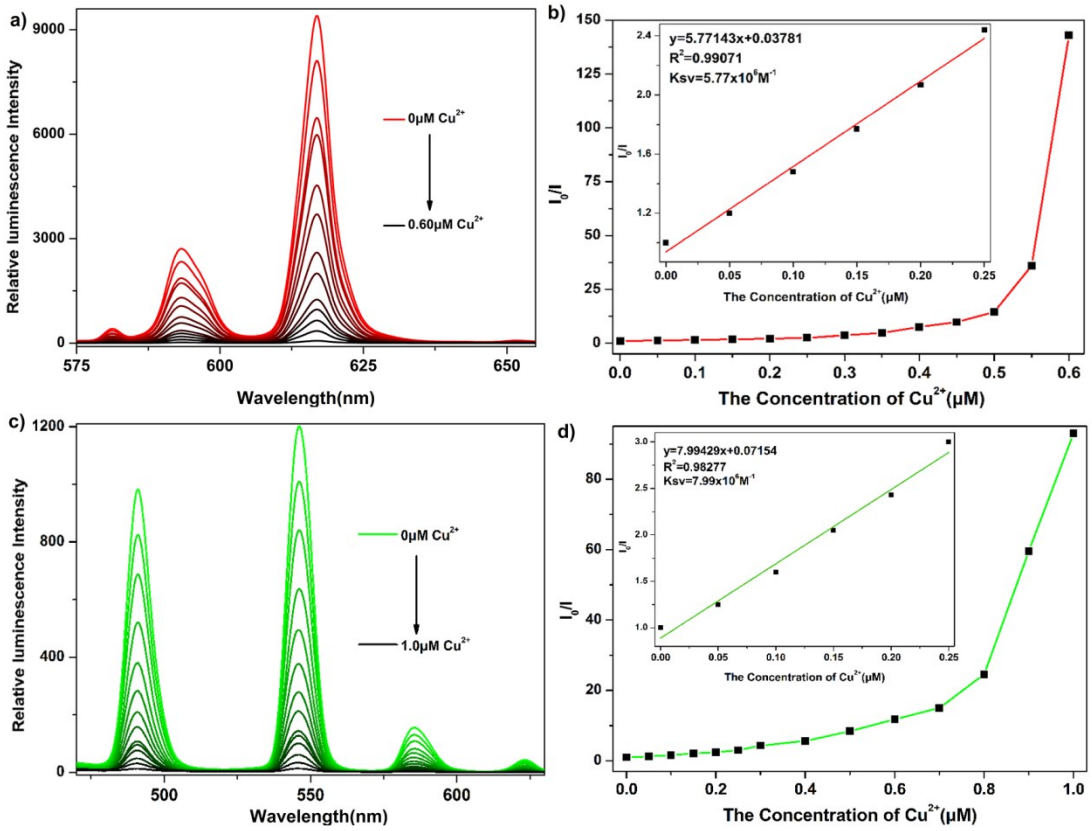

Fig. S15 a) The luminescence response of **LZG-Eu** to different concentrations of Cu^{2+}(0-0.60μM) in river water. b) The relationship between the I_0 / I Stern-Volmer diagram of **LZG-Eu** and the increase of Cu^{2+} concentration in river water. c) The luminescence response of **LZG-Tb** to different concentrations of Cu^{2+}(0-1.0μM) in river water. d) The relationship between the I_0 / I Stern-Volmer diagram of **LZG-Tb** and the increase of Cu^{2+} concentration in river water.

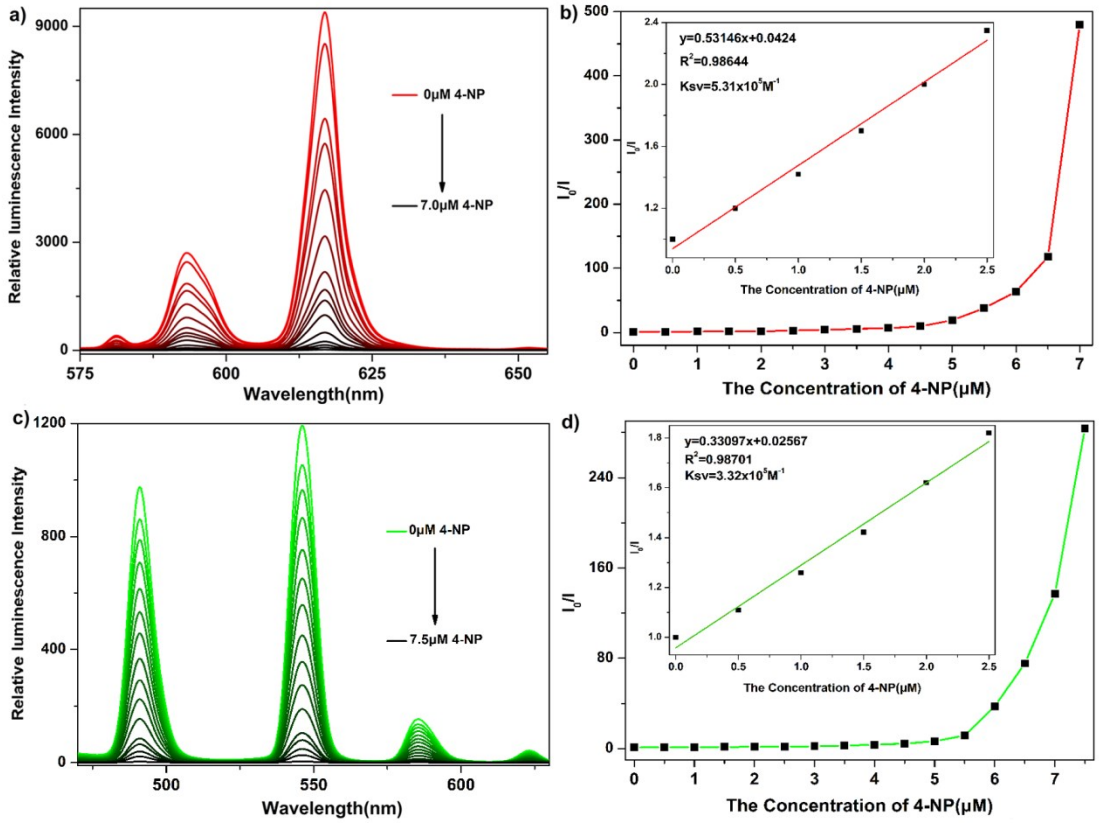

Fig. S16 a) The luminescence response of **LZG-Eu** to different concentrations of 4-NP(0~7.5μM) in river water. b) The relationship between the I_0/I Stern-Volmer diagram of **LZG-Eu** and the increase of 4-NP concentration in river water. c) The luminescence response of **LZG-Tb** to different concentrations of 4-NP(0~7.5μM) in river water. d) The relationship between the I_0/I Stern-Volmer diagram of **LZG-Tb** and the increase of 4-NP concentration in river water.

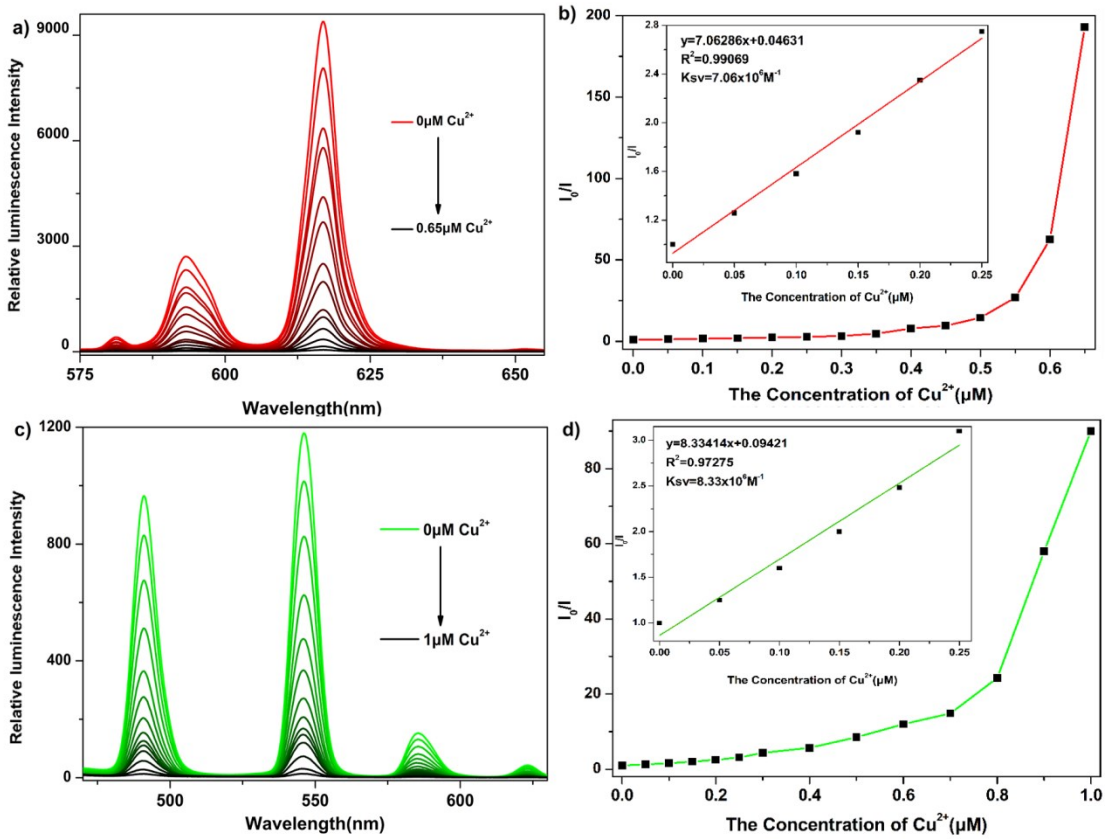

Fig. S17 a) The luminescence response of **LZG-Eu** to different concentrations of Cu^{2+}(0~0.65μM) in tap water. b) The relationship between the I_0/I Stern-Volmer diagram of **LZG-Eu** and the increase of Cu^{2+} concentration in tap water. c) The luminescence response of **LZG-Tb** to different concentrations of Cu^{2+}(0~1.0μM) in tap water. d) The relationship between the I_0/I Stern-Volmer diagram of **LZG-Tb** and the increase of Cu^{2+} concentration in tap water.

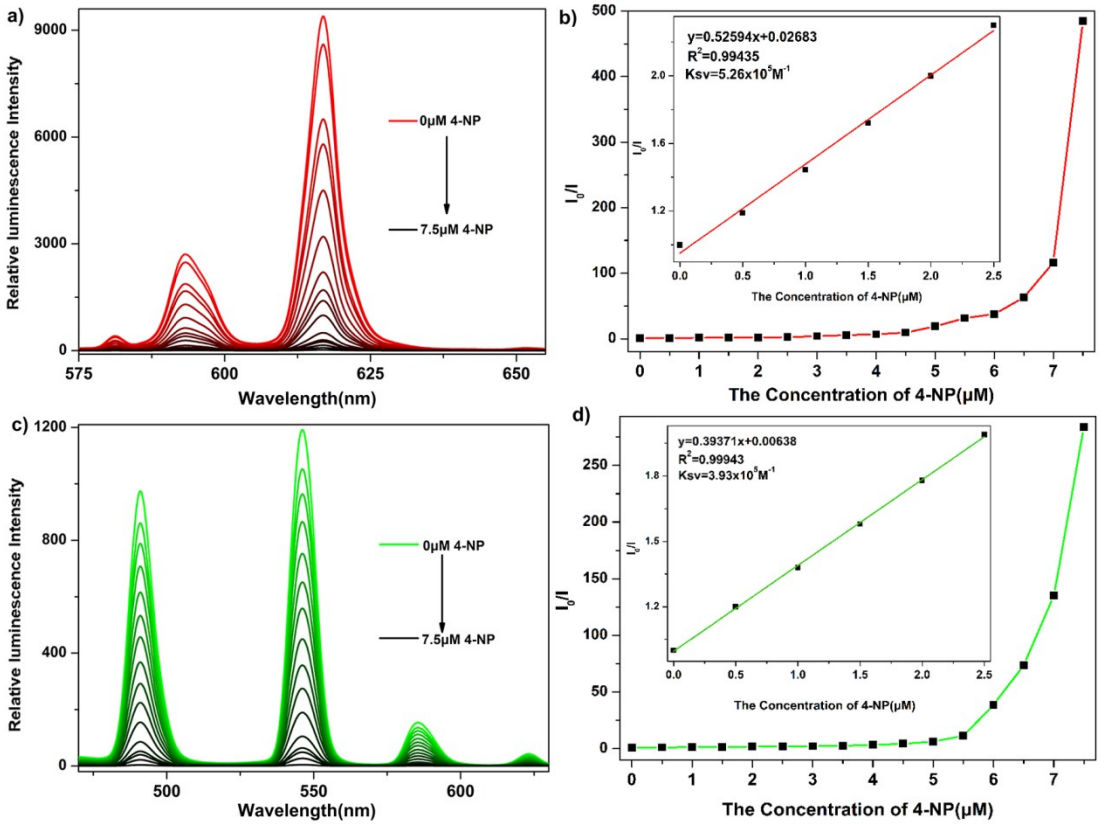

Fig. S18 a) The luminescence response of **LZG-Eu** to different concentrations of 4-NP(0~7.5μM) in tap water. b) The relationship between the I_0/I Stern-Volmer diagram of **LZG-Eu** and the increase of 4-NPconcentration in tap water. c) The luminescence response of **LZG-Tb** to different concentrations of 4-NP(0~7.5μM) in tap water. d) The relationship between the I_0/I Stern-Volmer diagram of **LZG-Tb** and the increase of 4-NP concentration in tap water.

Reference

1 G. M. Sheldrick, SHELXTL, Reference Manual: version 5.1: Bruker AXS; Madison, WI, 2014.

2 A. L. Spek, J. Appl.Crystallogr, 2003, **36,** 7.

3 DIAMOND. version 3.1; Crystal Impact: Bonn, Germany, 2004.